From form to function:
Morphology as a proxy for life history and population performance in fish

Victoria Dixon & Isabel M. Smallegange

School of Natural and Environmental Sciences, Newcastle University,
Newcastle upon Tyne, NE1 7RU, UK

Corresponding author: Isabel Smallegange, isabel.smallegange@newcastle.ac.uk

Keywords: Demography, Conservation, Growth-reproduction trade-off, Matrix model, Morphometrics, Pace-of-life

AUTHOR CONTRIBUTIONS

V.D. conceived the ideas and V.D. and I.M.S. designed the methodology; V.D. collected the morphology data, analysed the data and led the writing of the manuscript. Both authors contributed critically to the drafts and gave final approval for publication.

ACKNOWLEDGEMENTS

The authors thank Sol Lucas for support with analysing the data. ChatGPT-5 was used for language editing, grammar refinement and reference formatting.

DATA AVAILABILITY STATEMENT

Data and code used to analyse the data run the models in MATLAB and R, as well as the Appendices are available at Figshare: https://figshare.com/s/32350693789254b34ae4.

ORCID

Victoria Dixon: https://orcid.org/0009-0000-4831-6686

Isabel M. Smallegange: https://orcid.org/0000-0001-6218-7358

Abstract

1. Life history strategies emerge from trade-offs between growth, survival and reproduction and are key predictors of how populations respond to environmental disturbances. However, estimating these strategies typically requires detailed demographic data, which are unavailable for many species. Because morphological traits govern whole-organism performance, selection on ecological performance can link morphology with life history strategies. Morphological traits can thus be practical proxies for life history strategies, offering a scalable approach for data-deficient populations.
2. To test the hypothesis that morphological traits predict major life-history axes—and, by extension, population performance and resilience—via shared performance trade-offs, we parameterised dynamic energy budget integral projection models for 290 marine and freshwater fish species to quantify life history strategies and measured eight morphological traits from lateral-view photographs for each species. We used phylogenetically corrected principal component analysis to summarise life history strategies and morphological traits, and tested whether morphology predicts life history strategies, and whether either predicts population growth rate or demographic resilience.
3. Lateral size morphology, comprising body elongation, relative eye size and oral gape position predicted generation turnover depending on water column position, and predicted reproductive output depending on clade. Generation turnover, reproductive output and lateral size morphology predicted population growth rate and resilience, but population growth rate and resilience were not directly aligned, challenging common assumptions in fisheries management that treat them as interchangeable.
4. Our results support the hypothesis that morphologies linked to ecological performance scale up to shape demographic strategies, providing proof of concept that morphology can predict life-history strategies. They also highlight the potential to develop performance-based trait proxies for rapid, low-cost estimations of demographic vulnerability and recovery potential across data-poor fish populations—expanding the scope of life-history frameworks for fisheries management and conservation under increasing pressures from overfishing, habitat loss and climate change.

1 | INTRODUCTION

Life history strategies shape how species grow, survive, and reproduce—ultimately determining how they persist and adapt in a changing world (Stearns, 1992, 2000). These strategies emerge from fundamental trade-offs in allocation of limited resources among growth, survival and reproduction, shaped by evolutionary history and ecological context (Gaillard et al. 2016). Understanding where species fall along major life history axes provides powerful insights into their vulnerability to disturbance, potential for recovery, and long-term persistence (Salguero-Gómez 2017) — issues that are increasingly critical as global conditions change.

Two key axes capture much of this variation across taxa: the *fast–slow* continuum and the *parity* continuum (Gaillard, 1989; Bielby et al., 2007; Salguero-Gómez et al., 2016; Bakewell et al., 2020). Along the fast–slow continuum, slow-lived species mature late, reproduce less frequently and live longer, while fast-lived species reproduce early and often but have shorter lifespans (Pianka, 1970; Sæther, 1987). The parity continuum contrasts semelparous species, which invest all reproduction into a single event, with iteroparous species that reproduce multiple times (Salguero-Gómez et al., 2016; Healy et al., 2019). Species' positions along these continua have been used to predict their sensitivity to environmental change, invasions and extinction risk (Morrison and Hero, 2003; Salguero-Gómez, 2017; Paniw et al., 2018; Ozgul et al., 2024). Fast-lived species, for instance, are often assumed to recover more quickly from disturbance due to faster generation turnover, though this relationship is not universal (Rademaker, van Leeuwen and Smallegange, 2024). Nevertheless, such frameworks have become increasingly relevant for conservation, climate impact assessment and fisheries management (King and McFarlane, 2003; Carruthers et al., 2014; Pennino, Coll and Cerviño, 2023; Smallegange, Edwards and Attle, 2025).

The trade-offs that underpin life history strategies also manifest in morphological, behavioural and physiological traits (Reznick, Bryga and Endler, 1990; Violle et al., 2007). If these traits could reliably reflect a species' life history strategy, they would offer a scalable and cost-effective pathway to infer ecological performance and resilience, since functional trait data are easier to collect than demographic time series. Morphological traits are particularly promising because many remain stable throughout an individual's adult life, enabling robust cross-species comparisons. In plants, morphology–life-history links have been established at broad taxonomic scales, where traits related to stature, leaf economics and reproductive architecture mediate growth and survival trade-offs (Milla et al., 2008; Adler et al., 2013; Salguero-Gómez, 2017). But similar large-scale analyses are rare for other taxa (Stott et al., 2024). Morphological traits are directly linked to whole-organism performance (Lailvaux & Husak, 2014; Lailvaux & Husak, 2017), including locomotion efficiency, foraging success, predator avoidance and energy expenditure (Gatz 1979; Reznick et al. 1990; Violle et al. 2007). Because performance mediates survival, growth and reproduction, selection on ecological function should create consistent evolutionary associations between form and life-history strategy (Clements & Ozgul 2016; Laughlin et al. 2020). In fish, for example, traits that influence swimming hydrodynamics, visual foraging and feeding mechanics – such as body elongation, eye size and oral gape position – are therefore expected to covary with generation time, reproductive output and life-

history pace, particularly across environmental gradients where hydrodynamic and foraging-related selective pressures differ (Chea et al. 2021; Webb, 1984). But despite extensive work linking functional traits to demography in terrestrial taxa, particularly plants (Milla et al. 2008; Adler et al. 2013; Salguero-Gómez et al. 2017), large-scale tests of these links in fishes, or other aquatic taxa, remain rare.

This study tests the hypothesis that fish morphological traits, linked to swimming behaviour, food acquisition and predator avoidance, predict major life-history axes—and, by extension, population growth rate and resilience—via shared performance trade-offs. Their extraordinary morphological diversity arises from both ecological specialisation and strong phylogenetic constraints (Gatz, 1979; Salguero-Gómez et al., 2018), and morphological measurements can now be efficiently extracted from widely available lateral-view photographs (Brosse and Charpin, 2021). Yet, no study has systematically tested whether fish morphology predicts life history strategies across large phylogenetic and ecological scales. Moreover, fish life histories do not always conform to terrestrial models: slow-lived fish species often produce more, not fewer, offspring than fast-lived species (Jeschke and Kokko, 2009; Capdevila et al., 2020), and, when accounting for body size, aquatic species overall exhibit a faster pace of life than terrestrial ones (Capdevila et al., 2020).

To test our hypothesis, we parameterised Dynamic Energy Budget Integral Projection Models (DEB-IPMs; Smallegange et al., 2017) for 290 marine and freshwater species to model survival, growth and reproduction based on species-specific energy budgets and individual-level trade-offs in energy allocation (Kooijman, 2000; Smallegange and Lucas, 2025). From these models, we calculated a set of representative life history traits describing schedules of survival, growth and reproduction, and summarised them using a phylogenetically corrected principal component analysis (PCA) to identify the major axes of fish life history strategies. We applied the same approach to morphological data, using morphological ratios commonly applied in fish biology (Villéger et al., 2017; Brosse and Charpin, 2021) to derive composite morphological axes related to swimming behaviour, food acquisition and predator avoidance. We then assessed the influence of these composite morphological axes, along with phylogenetic ancestry, climate zone and water column position, on species' positions along the major life history strategy axes, to explore if selection acting on performance differs across environments and lineages. Finally, because life-history strategies mediate the demographic consequences of performance trade-offs, we tested whether species' positions along both life history and morphological axes predicted population growth and the speed of recovery from disturbance (demographic resilience). This approach demonstrates a novel application of modelling and analytical techniques to explore the relationship between morphology and life history — providing a pathway for scalable estimation of fish life histories and resilience to environmental change.

2 | METHODS

2.1 | Dynamic Energy Budget Integral Projection Model (DEB-IPM)

A DEB-IPM is a demographic model that uses eight life history parameters (Table 1) to capture the demographic rates of survival, growth, reproduction, and the relationship between parent and offspring sizes for females within a population (Smallegange *et al.*, 2017; Smallegange and Lucas, 2024). These demographic rates are derived from the simple version of the Kooijman-Metz model (1984). The Kooijman-Metz model assumes that organisms are isomorphic (individuals retain the same overall shape and proportions as they grow, resulting in external morphological similarity, even between individuals with differing phylogenies or biological roles), are born at length L_b, mature at length L_p and ingest food at a rate that is proportional to their experienced energy acquisition level. A feeding level $E(Y)$ represents the fullness of the animal's stomach from completely empty ($0 \geq E(Y) > 0.1$) to completely full ($0.9 \geq E(Y) \geq 1$) (Piet and Guruge, 1997). At $E(Y) = 1$, the highest feeding level, individuals grow to their maximum length (L_m) and reproduce at their maximum rate (R_m). As individuals feed and uptake energy, a constant fraction of assimilated energy is allocated to respiration (κ) to cover costs of maintenance and somatic growth. Any remaining energy is allocated to reproduction in adults or development of reproductive organs in juveniles. Note that R_m is proportional to $(1 - \kappa)$, whereas L_m is proportional to κ, which controls energy conservation. However, the role of κ in a DEB-IPM is mostly implicit, as κ is used as input parameter only in the starvation condition, whereas R_m and L_m are measured directly from data. Growth follows a von Bertalanffy curve characterised by its growth coefficient ($\dot{r}_B$). Individuals grow from year t to year $t + 1$ if they survive. Their survival chances are determined by mortality rates which differ for adults (μ_a) and juveniles (μ_j). To account for survival during the egg and larval phases, where the highest mortality occurs for ray-finned fish, R_m was multiplied by 0.001 for all actinopterygians (Rademaker, van Leeuwen and Smallegange, 2024).

2.2 | Parameterising the DEB-IPMs

We used the DEBBIES dataset (Smallegange and Lucas, 2024), which contains demographic trait data for 161 ectotherms including 3 actinopterygians and 158 chondrichthyans. We expanded this dataset by retrieving demographic data from FishBase (Froese and Pauly, 2013) and the wider literature (Figure 1). To this end, we developed a filtering method to search through all the entries in FishBase across multiple topics to create a list of species that were likely to have all the necessary demographic data (Appendix A: Filtering Method) (Froese and Pauly, 2013). The fraction of energy allocated to respiration (κ) values were found on the Add-my-Pet website or, if unavailable, assigned 0.8, which is accepted as a generic value for animals ('Add-my-pet', 2023). Length at puberty (L_p) and maximum length (L_m) were collected from species' summary pages (Froese and Pauly, 2013). Female length values were preferred over male ones. Typically, measurements were in total length (snout to end of caudal fin). Any values that were in fork length (snout to start of tail fork) or standard length (snout to start of precaudal fin) were converted to total length using the species-specific Length-Length tables

from FishBase (Froese and Pauly, 2013). Studies that used a greater sample size were preferred in instances of multiple conversion coefficients.

Maximum reported age (t_{max}) was also collected from the summary pages for use in mortality calculations (Froese and Pauly, 2013). Mortality rates were calculated using the same method as the DEBBIES dataset species for consistency. Adult mortality rate was calculated as $\mu_a = \frac{1}{[(t_{max}+t_\alpha)/2]}$ (Pardo *et al.*, 2016; Smallegange and Lucas, 2024), where age at maturity (t_α) was calculated as an average of the recorded observations (t_{max}) for females and unsexed entries from maturity studies pages on FishBase (Froese and Pauly, 2013). For juveniles, $\mu_j = -log\ (l_\alpha^{1/t_\alpha})$ where survival to maturity $l_\alpha = e^{-\mu_a(t_{max}-t_\alpha)}$. Unsexed data were included as female-only data were not available for all species. Male or mixed sex data were only used in the absence of other options. For most actinopterygians, the highest proportion of mortalities takes place during the egg and larval stages, so an additional survival factor was introduced into the reproductive rates as described below (Rademaker, van Leeuwen and Smallegange, 2024).

The Brody growth rate coefficient ($\dot{r}_B$) was sourced from the species-specific growth parameters available from FishBase (Froese and Pauly, 2013). Some of the FishBase coefficients were derived from equations where the infinite length was more/less than 1/3 of the maximum length – making them less reliable so using maximum observed age to calculate growth rate, ($\dot{r}_B = -log\ (1-0.95)t_{max}$), was tested as an alternative. A one-way analysis of variance (ANOVA) determined that using maximum age to find the coefficients produced significantly different values compared to the reliable growth rate values from FishBase ($F_{1,222}$=4.311, p=0.039), so all the FishBase values were retained for consistency (Froese and Pauly, 2013).

Maximum reproductive rate (R_m) was calculated using fecundity data (maximum number of eggs possibly produced across a female's lifetime) from the species' reproduction pages on FishBase (Froese and Pauly, 2013). Where multiple observations were recorded, an average of only the maximum values (including single values if a range was not present) was calculated. Maximum fecundity was then divided by the species' adult lifespan to represent maximum clutch size per year – unless the adult lifespan was less than 1 year then maximum fecundity was left unchanged. To capture egg and larval mortalities, reproductive rate was multiplied by 0.001 for all actinopterygians (Houde and Zastrow, 1993; Rademaker, van Leeuwen and Smallegange, 2024; Smallegange and Lucas, 2024).

Further species were added from Rademaker, van Leeuwen and Smallegange (2024). Four of our demographic parameters were available for 21 species (L_p, L_m, $\dot{r}_B$ and R_m). The information for the other parameter values was collected by following the protocols described above.

If a species was missing one trait value, either length at birth or reproductive rate, and there was another species of the same genus with a value present, then that value was used. Otherwise, species with missing values were removed from the dataset. These methods added 160 actinopterygians (21 from Rademaker, van Leeuwen and Smallegange (2024)) to the

demographic trait dataset totalling 321 species (158 chondrichthyans and 163 actinopterygians; species list in the Supplementary Material).

Finally, we chose to set the feeding level high at 0.9 across all species for consistency and to better demonstrate where species allocate their energy under realistic optimum conditions (.e.g, a feeding level of 0.8 is associated with natural, stable populations in reef manta rays (*Mobula alfredi*) (Smallegange *et al.*, 2017).

2.3 | Quantifying life history strategies

Using the parameterised DEB-IPMs, we derived eight representative life history traits based on schedules of survival, growth and reproduction (Table 1) (Salguero-Gómez *et al.*, 2016; Salguero-Gómez, 2017; Capdevila *et al.*, 2020) in MATLAB Version 24.2 (The MathWorks Inc, 2024) using the code in Smallegange & Lucas (2024). We also calculated the population growth rate (λ_0) for later use. To this end, we discretised each DEB-IPM (Smallegange and Lucas, 2024) by dividing the length domain Ω into 200 very small-width discrete bins, resulting in a matrix **A** of size 200x200, of which the dominant eigenvalue equals λ_0. Finally, we calculated demographic resilience as a damping ratio (ξ) with $\xi = \lambda_0 / \lambda_2$, where λ_2 is the highest subdominant eigenvalue of matrix **A** (Caswell, 2001; Capdevila *et al.*, 2020). Alternative metrics to capture resilience exist (simulated time-to-recovery or transient growth rates (Stott, Townley and Hodgson, 2011; Capdevila *et al.*, 2021), but for ease of comparison with previous studies, we used the damping ratio.

The results of the models were scanned for outliers before proceeding to the next stage of analysis. *Alosa sadipissima* was the only species to produce an NA value and was removed from the dataset. Despite introducing an egg/larval survival factor to reduce reproductive output, several species had abnormally high population growth rates and resilience. A further 23 species were removed as they met one or both of the following rejection criteria: $0.7 > \lambda_0 > 3.0$ or $\xi > 3.0$. The Greenland shark, *Somniosus microcephalus*, was also removed after visual inspection of the data due to its unusually high longevity – a precedent set in other studies (Lucas *et al.*, 2025; Smallegange and Lucas, 2024).

The life history traits were log-transformed and scaled ($\mu = 0$ and SD = 1) to meet principal component analysis assumptions before use in a phylogenetically corrected and length corrected principal components analysis (pPCA) (Revell, 2012) to identify life history strategy axes. Body length was corrected for in R by calculating the linear model residuals of the log-10 transformed life history traits and maximum body length, previously collected from FishBase, for each species (Gaillard, 1989; Froese and Pauly, 2013; R Core Team, 2024).

Phylogenetic corrections were made at the species level using the *phy.pca* function from the *phytools* library in R (Revell, 2012; Salguero-Gómez *et al.*, 2016; Paniw *et al.*, 2018; R Core Team, 2024). The phylogenetic tree was generated using the *rotl* package (version 3.1.0) to find each species' position on the Open Tree of Life (OTT) (Michonneau, Brown and Winter, 2016). The branch lengths of the tree inform on relatedness by scaling proportionally to the divergence times for clades and species. The pPCA linked phylogeny from the tree to the life history traits

through a modified covariance matrix. The pPCA also provided an estimate of Pagel's lambda (λ_p) – a scaling parameter for the phylogenetic correction between species from phylogenetic independence (0) to the species covarying proportionally to their shared evolutionary history (1) (Pagel, 1999; Freckleton, Harvey and Pagel, 2002). A further four species were excluded because they were not available from the OTT database: *Urobatis halleri*, *Dipturus intermedius, Osmerus dentex,* and *Osmerus mordax*.

PCAs were run with and without the phylogenetic and body length corrections to determine their influence on the structuring of life history strategies. An arbitrary cutoff value of 0.25 was set for λ_p as, below it, the impact of their shared evolutionary history was deemed limited (Lucas et al. 2025). The significance of the principal components axes was assessed using Kaiser's criterion (Kaiser, 1960).

2.4 | Collecting morphological trait data

Morphological data were collected from lateral view images by following the methodology from FISHMORPH (Brosse and Charpin, 2021). FISHMORPH is a database containing eight unitless ratios (Tables 2, 3) and body length, for 8,432 freshwater fish species (Brosse and Charpin 2021). These ratios are related to swimming efficiency (body elongation, body lateral shape, caudal fin throttling, pectoral fin position and pectoral fin size), prey/predator detection (relative eye size, vertical eye position), and prey capture mechanics (vertical eye position, oral gape position, jaw maxillary length) (Brosse and Charpin, 2021), and contribute to whole-organism performance which mediates survival and reproductive success. Therefore, these performance components are predicted to covary with species' positions along the fast–slow and parity life-history axes. We calculated these ratios for each of our remaining 290 marine and freshwater fish species from a series of measurements taken from lateral view images (see Appendix B). Rules for unusual morphologies were followed where applicable (Villéger *et al.*, 2010; Brosse and Charpin, 2021). FISHMORPH and its protocols were created for freshwater actinopterygians, so some adaptations were made to accommodate the chondrichthyans and seahorses into the same methodology (see Appendix B).

The fork in caudal fins is related to the individual's acceleration and manoeuvrability (Mouchet *et al.*, 2019). To explore tail shape in greater depth, an additional ratio was designed called caudal forkedness (CFk) (Table 3). This ratio is calculated by dividing the distance from the start of the caudal fin to the end point that divides the upper and lower lobes (along the lateral line of the spine) by the distance from the start of the caudal fin (along the top of the body) to the tip of the upper lobe (Table 2). Fins that are rounded have a value less than one and fins that have a strong fork have a value greater than one. As this ratio is not included in FISHMORPH and every ratio is required to be related to each other, every species had their values taken from images and not from the database. In the absence of a caudal fin, CFk was set to zero to represent a pointed tail.

Research grade photographs were found online primarily from iNaturalist (iNaturalist, 2023), FishBase (Froese and Pauly, 2013), institutional websites (i.e. museums, government organisations), or from the personal websites of specialists (image references available in

Supplementary Material). All images were available under fair dealing copyright law or had permission given for use in this work. As the life history data is modelled on females of the species, images of females were preferred in cases where extreme sexual dimorphism was known. The largetooth sawfish, *Pristis pristis*, is an exception where a diagram was used instead. Two species had no suitable photographs or diagrams available from any of these sources – *Pristis clavata* and *Sphyrna zaegna*. Their life history data is still available in the raw data file (see Supplementary Material), but they were not included in further analyses.

Images were uploaded to ImageJ 1.54p in a browser and measured in pixels (Schneider, Rasband and Eliceiri, 2012). Ratios were calculated following FISHMORPH (Tables 2, 3) (Brosse and Charpin 2021). Replicates were measured for several species from different pictures to assess intra-specific variability. The resultant ratios for each replicate were averaged and used as the entries for those species. Due to the introduction of a new ratio partway through collection, images were entirely re-measured to create data files that included the new caudal fork data. The difference between the former and newer measurements of body length never exceeded fifteen pixels which demonstrates consistency in measurement technique.

2.5 | Quantifying composite morphological axes

Due to the similarity between some of the traits represented by the morphological ratios, a Pearson's correlation test was run to determine if ratios covaried before conducting the phylogenetically corrected PCA (see Appendix C). The ratios that had the highest associations with each other were relative maxillar length (RMl) and oral gape position (OGp) as well as caudal forkedness (CFk) and caudal peduncle throttling (CPt). OGp was retained as it was available for more species than RMl. CFk was retained instead of CPt to test the applicability of a new caudal ratio (Mouchet *et al.*, 2019). The remaining traits were log-transformed and scaled to meet the PCA assumptions.

We then applied dimension reduction via phylogenetically corrected PCA to extract composite morphological proxies for swimming, foraging and positioning performance, which were then tested against life-history strategy axes. As Pagel's lambda was high for the life history pPCA, we decided to include phylogenetic corrections in the morphological PCAs as well to identify the main composite morphological axes. The morphological trait data were scaled (μ = 0 and SD = 1). The same tree from the life history pPCA was used. Linear model residuals of square root-transformed traits against log-transformed body length were used for the length corrected pPCA, as log-10 transformations were unsuitable for the trait corrections. The axes were assessed using a Kaiser's criterion (Kaiser, 1960).

The results of the morphological PCA are reported here, as the axes - named according to their strongest trait associations – serve as inputs for the main analyses (see below). Pagel's lambda was high (λ_p=0. 99), demonstrating a high phylogenetic signal (Pagel, 1999). A qualitative check demonstrated that trait loadings were different between length corrected pPCA and non-length corrected pPCA so the former was used. The final morphological pPCA was phylogenetically and length corrected. The first three axes were retained from the morphological pPCA because their eigenvalues were higher than unity (1.87, 1.69, and 1.38 respectively). The three axes

cumulatively explaining 61.93% of the total variance (Table 3: M-pPC1 23.42%, M-pPC2 21.15%, and M-pPC3 17.35%). Body elongation (BEl), relative eye size (REs), and oral gape position (OGp) all loaded negatively onto M-pPC1 (Table 3). As M-pPC1 increases, species have deeper bodies, smaller eyes and a lower mouth position relative to their head depth. M-pPC1 is therefore referred to as "*lateral size morphology*". Body elongation (BEl) loaded negatively onto M-pPC2, but oral gape position (OGp) and pectoral fin size (PFs) loaded positively (Table 3). As M-pPC2 moves from negative to positive scores, species have deeper bodies with larger pectoral fins and a higher mouth position. This trait combination can be associated with acceleration and agility so M-pPC2 will be referred to as "*locomotory morphology*". For M-pPC3, vertical eye position (VEp) and pectoral fin vertical position (PFv) both loaded negatively (Table 3). As M-pPC3 increases species have eyes in lower positions relative to their heads and lower pectoral fins relative to their trunks. M-pPC3 traits can be associated with position in the water column, relative to their food and predators, and will be referred to as "*positioning morphology*". Body lateral size and caudal fin forkedness did not load onto the first three axes (Table 3).

2.6 | Testing which morphological traits predict life history strategy

To test our hypothesis that morphological traits predict major life-history axes, we assessed whether composite morphological axes representing hydrodynamic form (lateral size morphology), locomotor capability (locomotory morphology), and habitat positioning relative to prey and predators (positioning morphology) covaried with species' positions along the fast–slow (generation turnover) and reproductive-output axes. We further tested whether these relationships were mediated by ecological context (water column position and climate zone) or phylogenetic ancestry (clade), consistent with predictions that selection acting on performance differs across environments and lineages.

Using data from FishBase, species were divided into broad categories describing the climate zone they are most frequently found in: deep-water (>200m), polar, temperate, and tropical (combined with subtropical) (Froese and Pauly, 2013). Similarly, FishBase was used for species' most frequented water position: deep-water (>200m), seafloor, pelagic, and reef (Froese and Pauly, 2013). Species' clades were broadly divided into ray-finned fish, sharks and rays/skates. The influences of climate zone, water position, clade, morphology and their interactions on life history strategies were tested using two General Linear Models (GLMs) using base R (R Core Team, 2024). The response variables were the life history principal component scores of either axis, and the predictor variables were climate zone, water position, clade and each of the morphological principal component (PC) scores (lateral size morphology, locomotory morphology, and positioning morphology). We excluded the interaction between climate zone and water column position because of overlapping categories among deep-water species and insufficient data for certain combinations of these variables (for example, the dataset contained no polar reef species). For both GLMs, the model assumptions of Gaussian errors and homoscedasticity were confirmed by visually inspecting the residual and Q-Q plots in R (R Core Team, 2024). In stepwise regression, insignificant interactions were removed from the models. Higher order interactions were removed first until only significant interactions and

fixed factors remained. Significance of interactions were determined by comparing each reduced model with the fuller one it is nested in, using ANOVA tests. Terms were removed if the p-value exceeded 0.05.

Because life-history strategies mediate the demographic consequences of performance trade-offs, we evaluated whether morphological predictors of life history strategy scaled to population growth rate and demographic resilience. To this end we applied GLMs to test if the life history principal components scores, and their interaction, predict population growth rate (λ_0) and species' resilience (ξ) using base R (R Core Team, 2024). Additionally, GLMs were used to test if any of the morphological PC scores or their interactions predict population growth rate and species' resilience. Even though PCA assumes that the principal components for life history strategy or morphology are uncorrelated, this assumption pertains to the original data's variance structure (Gaillard, 1989). Growth rate and resilience, the response variables, were both log-transformed. For both GLMs, the model assumptions of Gaussian errors and homoscedasticity were confirmed by visually inspecting the residual and Q-Q plots in R (R Core Team, 2024). If interactions between the PC scores were non-significant, they were removed by stepwise regression – removing higher order interactions first until only significant interactions and fixed factors remained, using ANOVA tests to determine significance of interactions ($p<0.05$). ANOVA tests were also used to report the influence of fixed factors. Where this was not possible due to the model becoming oversaturated, we report their parameter estimate, standard error and associated test statistics.

3 | RESULTS

3.1 | Major life history axes to describe variation in life history traits

After removing outliers or species with missing data, life history traits of 290 species were analysed (Figure 1A). Pagel's lambda was higher than the cut-off value of 0.25 (λ_p=0.98), indicating that the phylogenetic signal was strong (Pagel, 1999). A qualitative check of the trait loadings between the pPCA and the length corrected pPCA revealed differences of which axes the life history traits loaded onto. We thus proceeded with the phylogenetically and length corrected pPCA, referred to as the LH-pPCA. Two LH-pPC axes cumulatively explained 73.14% of the total variance in life history traits (Table 1: LH-pPC1 41.09%, LH-pPC2 32.04%), as their eigenvalues were higher than unity (3.287 and 2.563, respectively). Generation time (T), mean age at maturity (L_α; note that L_α is equivalent but not computationally the same as t_α, the observed age at maturity used above to calculate juvenile and adult mortality rates), progressive growth (γ), and mature life expectancy (L_ω) all loaded negatively onto LH-pPC1 whereas mean recruitment success (ϕ) loaded positively (eigenvalue<0.05) (Table 1). These traits are strongly associated with *generation turnover*. As LH-pPC1 scores increase, our species show shorter lifespans and greater generation turnover (Figure 1B). For LH-pPC2, mean age at maturity (L_α), mature life expectancy (L_ω), and net reproductive rate (R_0) loaded positively whereas retrogressive growth (ρ) loaded negatively onto LH-pPC2 (Table 1). These traits are strongly associated with *reproductive output*. As LH-pPC2 scores move from negative to

positive, species produce more offspring (Figure 1B). Degree of iteroparity (*S*) did not load onto either of the first two axes.

3.2 | Does morphology predict generation turnover?

Consistent with our hypothesis that traits related to swimming and foraging performance covary with life-history speed, lateral size morphology significantly predicted the generation turnover LH-pPC scores, but differently at different water positions (two-way interaction: $F_{3, 269}$=3.3864, p=0.0186). With increasing lateral size morphology, deep-water species had a lower generation turnover whereas species from all other depths had a higher generation turnover (Figure 2). The interaction between water position and clade also significantly impacted generation turnover ($F_{6, 269}$=2.2039, p=0.0429) Deep-water species had a lower generation turnover than other water positions across all clades, although the difference was most pronounced for the rays/skates (Figure 3A). Climate zone significantly predicted generation turnover as well ($F_{3, 269}$=9.4796, p<0.001). Deep-water species had significantly lower generation turnover than species in all other climate zones (Figure 3B). Polar species tended to have faster generation turnover than deep-water species but slower than temperate or tropical species (Figure 3B). All other interactions did not predict species' generation turnover: climate zone × positioning morphology ($F_{2, 243}$=0.8474, p=0.4298), climate zone × locomotory morphology ($F_{3, 245}$=1.3128, p=0.2708), climate zone × lateral size morphology ($F_{3, 248}$=0.8677, p=0.4584), water position × positioning morphology ($F_{3, 251}$=0.3993, p=0.7536), water position × locomotory morphology ($F_{2, 254}$=1.3458, p=0.26), clade × positioning morphology ($F_{2, 257}$=0.7117, p=0.4918), clade × locomotory morphology ($F_{3, 259}$=0.3059, p=0.7367), clade × lateral size morphology ($F_{3, 261}$=2.3399, p=0.0983), and clade × climate zone ($F_{6, 263}$=1.937, p=0.0752). Generation turnover was also not significantly impacted by locomotory morphology ($F_{1, 269}$=1.6508, p=0.2) or positioning morphology ($F_{1, 269}$=0.6279, p=0.4288). For the other fixed factors, the model became over saturated, so instead test statistics are reported for lateral size morphology (estimate=1.5913, std. error=0.6816, t=2.335, p=0.0203), water positions including pelagic (estimate=-0.0221, std. error=0.1701, t=-0.130, p=0.8964), reef (estimate=-0.1167, std. error=0.1734, t=-0.673, p=0.5013), and seafloor (estimate=-0.2226, std. error=0.1594, t=-1.397, p=0.1636), as well as the clades: rays/skates (estimate=-0.6308, std. error=0.2985, t=-2.113, p=0.0355) and sharks (estimate=0.0110, std. error=0.1518, t=0.073, p=0.9419).

3.3 | Does morphology predict reproductive output?

If offspring production depends on energetic acquisition and allocation strategies that are shaped by foraging mode, locomotor performance and predator–prey interactions, we tested whether composite morphological axes linked to these performance traits predicted reproductive output across fish clades. In partial support of this prediction, the interaction between clade and lateral size morphology significantly predicted reproductive output LH-pPC scores ($F_{2, 274}$=3.1796, p=0.0431). As lateral size morphology increased, reproductive output decreased in the ray-finned fish whereas it increased for the elasmobranchs (Figure 4A). The interaction between clade and locomotory morphology also significantly predicted reproductive output ($F_{2, 274}$=5.5527, p=0.0043). As locomotory morphology increased,

reproductive output decreased in the ray-finned fish and increased in the elasmobranchs (Figure 4B). Positioning morphology significantly predicted reproductive output ($F_{1, 274}$=6.6295, p=0.01056). As positioning morphology increased, vertical eye and pectoral fin positions were lower and reproductive output decreased across all species (Figure 4C). Clade was also an independent predictor ($F_{2, 274}$=15.586, p<0.001): ray-finned fish had the highest average reproductive output, followed by rays/skates and then sharks. No other interactions predicted reproductive output: climate zone × positioning morphology ($F_{2, 243}$=0.7296, p=0.4832), climate zone × locomotory morphology ($F_{3, 245}$=2.5782, p=0.0543), climate zone × lateral size morphology ($F_{3, 248}$=0.8445, p=0.4707), water position × positioning morphology ($F_{3, 251}$=2.3392, p=0.0739), water position × locomotory morphology ($F_{3, 254}$=2.4261, p=0.06608), water position × lateral size morphology ($F_{3, 257}$=0.5888, p=0.6229), clade × positioning morphology ($F_{2, 260}$=0.5617, p=0.571), clade × water position ($F_{4, 262}$=1.4914, p=0.1813), and clade × climate zone ($F_{6, 268}$=0.3983, p=0.8799). The following single factors were retained but were not significant predictors of reproductive output: positioning morphology ($F_{1, 274}$=6.6295, p=0.0156), climate zone ($F_{3, 274}$=1.8734, p=0.1343), clade ($F_{2, 274}$=15.586, p<0.001), and water position ($F_{3, 274}$=0.3042, p=0.8224). Lateral size morphology and locomotory morphology could not be reported on with ANOVA tests because the model became oversaturated. Instead, we report their test statistics from the final model: lateral size morphology (estimate=-0.3667, std. error=0.2798, t=-1.311, p=0.1910), locomotory morphology (estimate=-0.4356, std. error=0.2326, t=-1.873, p=0.0622).

3.4 | Do life history strategies or morphology predict population growth rate and resilience?

3.4.1 | Population growth rate

Generation turnover and reproductive output LH-pPC scores had a significant interactive effect on population growth rate ($F_{3, 286}$=583.36, p<0.001). At high reproductive outputs, increasing generation turnover predicted higher population growth rates whereas at low reproductive outputs increasing generation turnover had little impact on population growth rate which remained low (Figure 5A). Population growth rate was significantly predicted by generation turnover ($F_{1, 286}$=418.7, p<0.001) as well as reproductive output ($F_{1, 286}$=436.65, p<0.001).

In case of the morphological pPC scores, lateral size morphology significantly predicted population growth rate ($F_{1, 286}$=7.8471, p=0.0054). As species demonstrated greater body depth relative to their length, smaller eyes and lower oral gape positions, growth rates were lower (Figure 6A). Positioning morphology was also independently a significant predictor of population growth rate ($F_{1, 286}$=10.75, p=0.0011). Fish with lower vertical eye and pectoral fin positions had lower population growth rates (Figure 6B). No interactions were significant: lateral size morphology × locomotory morphology × positioning morphology ($F_{1, 282}$=0.5794, p=0.4472), locomotory morphology × positioning morphology ($F_{1, 283}$=0.7777, p=0.3786), lateral size morphology × positioning morphology ($F_{1, 284}$=0.19, p=0.6632), and lateral size morphology

× locomotory morphology ($F_{1, 285}$=0, p=0.0966). Locomotory morphology was also not significantly predictive ($F_{1, 286}$=0.0381, p=0.8453).

3.4.2 | Population resilience

Generation turnover and reproductive output LH-pPC had a significant interactive effect on population resilience ($F_{3, 286}$=51.009, p<0.001). At high generation turnover, resilience was predicted to be higher for species with lower reproductive outputs whereas at low generation turnover, resilience was predicted to be low regardless of reproductive output (Figure 5B). Population resilience was predicted by generation turnover ($F_{1, 286}$=124.8, p<0.001) as well as reproductive output ($F_{1, 286}$=14.508, p<0.001).

Only lateral size morphology PC scores independently predicted population resilience from the morphological trait axes ($F_{1, 286}$=7.6771, p=0.0059). As species' body depths increased and relative eye sizes and oral gape positions decreased, population resilience was predicted to decrease (Figure 6C). All interactions were insignificant and were removed from the model: lateral size morphology × locomotory morphology × positioning morphology ($F_{1, 282}$=0.243, p=0.6224), locomotory morphology × positioning morphology ($F_{1, 283}$=1e-04, p=0.994), positioning morphology × lateral size morphology ($F_{1, 284}$=0.3839, p=0.536), and lateral size morphology × locomotory morphology ($F_{1, 285}$=0.1154, p=0.7344). Population resilience was not significantly predicted by either locomotory morphology ($F_{1, 286}$=0.4351, p=0.51) or positioning morphology ($F_{1, 286}$=3.198, p=0.0747).

4 | DISCUSSION

Here, we tested the hypothesis that fish morphological traits linked to swimming behaviour, food acquisition and predator avoidance predict major life-history axes—and, by extension, population performance and resilience—via shared performance trade-offs. Especially the consistent association between lateral size morphology and generation turnover across environments supports our hypothesis and illustrates how hydrodynamic trade-offs translate into demographic strategies. We also found that morphology, generation turnover and reproductive output all influenced population growth rate and demographic resilience, yet in different ways, indicating that these axes capture distinct aspects of population performance rather than interchangeable ones. Notably, population growth rate did not map directly onto resilience, challenging a common assumption in conservation and fisheries management that fast population growth implies greater resilience to disturbance.

4.1 | Lateral size morphology as a predictor of generation turnover and fish performance across water positions

As predicted, a species' lateral size morphology linked to generation turnover. However, this relationship depended on a species' position in the water column, confirming how life history speed is mediated by ecological context (water column position and climate zone in this instance) (Kelly et al. 2021; Webb, 1984). In stable environments, generation time is often used

as a measure of a species' position along the slow–fast life-history continuum (Charlesworth, 1994; Heppell, Caswell & Crowder, 2000; Oli & Dobson, 2003; Gaillard et al., 2005; Stahl & Oli, 2006). Here, however, we foundd that a deeper body, smaller eyes relative to head depth, and a lower mouth position are associated with higher generation turnover in deep-water habitats, but lower generation turnover in pelagic, reef, and seafloor habitats. This pattern indicates that generation turnover does not consistently track life-history speed; rather, its relationship with morphology depends on where species live in the water column.

Lateral size morphology also predicted both population growth rate and resilience, with both increasing as fish exhibited deeper bodies, smaller eyes relative to head depth and lower mouth positions. This supports our premise that morphology not only predicts major life-history axes, but, by extension, population performance and resilience via shared performance trade-offs. The applications of morphology as a proxy for resilience to environmental disturbance could extend into accessible, cost-effective stock estimations. Indeed, many commercial fisheries have relied on intrinsic growth rate to estimate maximum sustainable yield (MSY), from the classic Gordon–Schaeffer model (Gordon, 1954) to more recent approaches such as abundance MSY (Froese et al., 2020). The American Fisheries Society formalised this link in 1996, categorising species with high growth rates and generation turnover as highly resilient (Musick, 1999; Punt, 2000). Yet, our results challenge this assumption: species with the highest population growth rates were not necessarily the most resilient. Instead, the most resilient species tended to have high generation turnover but low reproductive output. This implies that current fisheries assessments may overestimate the resilience of highly reproductive species and underestimate that of species with lower reproductive output, potentially skewing conservation priorities and leading to overexploitation under the false assumption of rapid recovery potential. However, our interpretation warrants caution, as the measure of resilience used here, the damping ratio, has known limitations. It captures how quickly a population returns to equilibrium after disturbance (Caswell, 2001) but ignores the initial population structure and cannot predict real recovery times (Stott, Townley & Hodgson, 2011). Further exploration using alternative resilience metrics, such as relative transient dynamics (Stott, Townley & Hodgson, 2011; Capdevila et al., 2021), is needed to determine whether this discrepancy reflects a methodological artefact or a genuine ecological pattern.

Selection on ecological function can create consistent evolutionary associations between form and life-history strategy, because performance mediates survival, growth and reproduction (Clements and Ozgul 2016; Laughlin et al. 2020). But what ecological function drives the association between morphology and generation turnover? In pelagic, reef, and seafloor habitats, lower generation turnover is associated with deeper bodies, smaller eyes and lower mouths. Although laterally compressed bodies incur greater drag, they enhance manoeuvrability, conferring advantages in predator evasion and prey capture (Howe, 2022), and can deter gape-limited predators (Brönmark & Miner, 1992; Nilsson, Brönmark & Pettersson, 1995). These benefits may lead to longer lifespans and thus slower generation turnover. In contrast, deep-water species show the opposite trend: lower generation turnover is linked to more elongate bodies, larger eyes and higher mouths. Below 200m, low light and high pressure select for energy-efficient, elongate morphologies adapted for slow, steady swimming

(Seibel, Thuesen & Childress, 2000; Tytell et al., 2010; Neat & Campbell, 2013). Larger eyes enhance light sensitivity, improving detection of prey, predators, or conspecifics (Land, 1981; Myers et al., 2019), without the visibility costs that such traits impose in illuminated habitats (Andersson, Scharnweber & Eklöv, 2024). Thus, opposing relationships between morphology and generation turnover likely arise because different depths impose contrasting selective pressures—balancing hydrodynamics, energy efficiency, and predator–prey interactions.

4.2 | Morphology as a predictor of reproductive output and fish performance across clades

Similar to the links between morphology and generation time, the question is what ecological functions shape how morphology connects to reproductive output across different clades? Along the lateral size morphology axis, sharks and ray-finned fish with deeper bodies, lower mouths and smaller eyes occupy the higher end of the spectrum. This morphology is characteristic of demersal feeders, where enhanced manoeuvrability is advantageous in clustered habitats and large eyes are less critical because prey are often sedentary benthic invertebrates (Linsey & Collin, 2007; Gleiss, Potvin & Goldbogen, 2017; Howe, 2022). At the opposite end of the axis are sharks and ray-finned fish with elongated bodies and larger eyes positioned in shallower heads: a morphology typical of pelagic hunters, which benefit from reduced drag and improved visual tracking of mobile prey such as fish and cephalopods (Linsey & Collin, 2007; Gleiss, Potvin & Goldbogen, 2017). The positioning of rays and skates along this same axis reflects intra-clade differences: skates, with their shorter tails and reduced body elongation, plot higher than rays. Benthic-associated sharks and skates tend to exhibit higher reproductive output than pelagic-associated species because they are primarily oviparous (egg-laying), whereas many pelagic elasmobranchs are viviparous (live-bearing) (Katona et al., 2023). Consistent with the well-known trade-off between litter size and offspring size (Hussey, 2009; Sibly et al., 2018; Katona et al., 2023), oviparous elasmobranchs produce more but smaller offspring, while viviparous species produce fewer but larger ones. In pelagic systems, larger offspring have a greater chance of survival because of intense predation and limited refuges (Hussey, 2009; Sibly et al., 2018). This trade-off between survival/growth and reproduction explains the lower reproductive output of pelagic elasmobranchs. However, ray-finned fish show the opposite pattern: pelagic-associated species display higher reproductive outputs than benthic-associated ones. These species maximise recruitment success via broadcast spawning, releasing vast numbers of small eggs to offset high predation and resource limitation in the pelagic zone (Elgar, 1990; Winemiller & Rose, 1993; Sibly et al., 2018). Thus, the lateral morphology axis appears to capture a shared performance trade-off between offspring size and litter size that transcends clades, even though those trade-offs are realised through different reproductive strategies.

The link between morphology and reproductive output observed here is indirect, mediated through established trade-offs among growth, survival and reproduction. While the lateral size axis clearly reflects this pattern, relationships along the locomotory and positioning axes were weaker or reversed. For example, elongation along the locomotory axis did not consistently predict lower reproductive output, suggesting that different trade-offs between swimming

behaviour and fecundity operate across species. Likewise, the relationship between vertical eye and pectoral-fin position and reproductive output hints at behavioural or ecological trade-offs related to prey and predator positioning in the water column, but these mechanisms remain speculative. Notably, while lateral size morphology predicted both population growth rate and resilience, positioning morphology predicted only growth rate, and locomotory morphology predicted neither. This suggests that morphology–reproduction–performance linkages are more diffuse and context-dependent than those between morphology and generation turnover. One likely reason for this is that the morphological traits used in this study are functionally related to swimming, foraging and predator–prey interactions, but only indirectly to reproduction. Incorporating explicitly reproductive morphological traits (e.g. gonad size, oviduct morphology, clasper dimensions) could clarify these relationships, though such traits are often internal or not visible from lateral images. A more practical avenue may be to include additional life-history traits that capture reproductive trade-offs directly, such as offspring size, egg size or degree of parental care (Hussey, 2009; Sibly et al., 2018). Integrating these would better define the morphological correlates of reproductive strategy and improve the predictive power of morphology for life-history and population performance models.

4.3 | Can morphology serve as a proxy for population performance?

A key motivation for this work was to test if fish morphological traits predict major life-history axes, and, by extension, predict population performance and resilience. Life history frameworks are powerful tools for understanding demographic resilience and vulnerability, yet their application is limited by the intensive data requirements of estimating individual-level demographic rates across full life cycles (Salguero-Gómez et al., 2018; Smallegange & Lucas, 2024). In contrast, morphological traits can be measured rapidly, even from photographs or museum specimens, making them appealing candidates for large-scale functional assessments (Schultz et al., 2020; Zhang & Fouhey, 2022). Recent frameworks show that functional traits can be used to estimate demographic performance across species (Siefert & Laughlin, 2023) and that trait positions scale up to demographic outcomes (Wieczynski et al., 2021). If morphology reliably captures a species' position along the life history continuum, and by extension, its expected population dynamics, it could greatly expand the taxonomic and spatial scope of life history approaches in ecology and conservation.

However, our findings suggest that the relationship between morphology and population performance is complex and context-dependent. Morphology predicted generation turnover and reproductive output, but these relationships differed among clades and environments so they did not translate directly into consistent predictions of population growth or resilience. This finding echoes a broader theme in trait–demography research: phenotypic traits, while often correlated with demographic rates, do not necessarily encapsulate the underlying life history processes that drive population performance (Clements & Ozgul, 2016). For example, body size has long been used as a proxy for performance or fitness, yet shifts in size distributions can arise through different demographic mechanisms in species with contrasting life histories (Smallegange & Berg, 2019). Fast life history species often show changes in body size distributions driven by altered reproduction, whereas slow life history species are more

strongly shaped by variation in individual growth (Clements & Ozgul, 2016). Morphological correlates of performance are therefore contingent on which underlying processes dominate population dynamics. There is thus a need for taxon-specific examination of how morphology maps onto life-history strategies, because identifying the performance-driven mechanisms linking form to demography is essential both for understanding the evolutionary diversification of life histories and for developing reliable trait-based predictions of population resilience.In this study, morphology predicted population growth rate and resilience through different pathways: generation turnover and reproductive output interacted to influence each, but not in parallel ways. This decoupling implies that morphological traits can indicate certain components of performance, such as turnover potential or reproductive capacity, but not the emergent outcome of resilience, which integrates multiple performance trade-offs. Consequently, while morphology may provide a first approximation of where a species lies along the performance spectrum, it cannot yet substitute for detailed demographic information when assessing vulnerability or recovery potential. For example, the concept of trait networks illustrates how trait-trait combinations, rather than single traits, mediate resilience (Swenson et al., 2019). Nevertheless, the use of morphology as a proxy remains a promising direction, particularly for data-poor taxa. Morphological datasets are expanding rapidly through digital archives, museum collections and citizen science imaging, offering opportunities to link phenotypic variation to demographic and ecological outcomes across broad phylogenetic and environmental gradients (Gonçalves Souza et al., 2023). Future progress will depend on explicitly coupling morphological traits to the demographic mechanisms that underlie population performance—identifying, for instance, which combinations of shape, size and organ placement reflect trade-offs in survival, growth, and reproduction (Salguero Gómez et al., 2018). Integrating these approaches within hierarchical trait–demography frameworks could yield generalizable models capable of predicting resilience or recovery potential for species lacking detailed demographic data (Siefert et al., 2023).

5 | CONCLUSION

Ultimately, this study provides proof of concept that morphology—particularly lateral size morphology tied to hydrodynamic constraints—can predict key life history axes and elements of population performance across diverse fish taxa. Body elongation, relative eye size and oral gape position emerged as strong correlates of generation turnover, linking water column position and swimming behaviour to life history strategy. These findings suggest that hydrodynamic forces may act as a unifying selective pressure shaping both morphology and demography in aquatic systems. As fish populations face accelerating pressures from overfishing, climate change and habitat loss, developing robust morphological proxies for life history and resilience will be essential. Identifying a suite of externally measurable traits that reliably predict population performance would allow life history frameworks to be applied to many more data-deficient species—providing a scalable pathway to anticipate and mitigate biodiversity loss in changing aquatic ecosystems.

CONFLICT OF INTEREST STATEMENT

The authors do not have any conflict of interest to report.

ETHICAL APPROVAL

The work used published data on vertebrates that do not need ethical permissions.

STATEMENT ON INCLUSION

This study prioritises broad taxonomic and ecological representation by including 290 marine and freshwater fish species spanning multiple clades, water column positions and climate zones. While no human subjects were involved, we acknowledge the importance of diversity in scientific collaboration and data sources. Future work should continue to expand inclusion of understudied regions and species to ensure equitable representation in global ecological and conservation research.

REFERENCES

'Add-my-pet' (2023). Available at: www.debtheory.org (Accessed: 7 September 2025).

Adler, P. *et al.* (2013) 'Functional traits explain variation in plant life history strategies', *Proceedings of the National Academy of Sciences: Biological Sciences*, 111(2), pp. 740–745.

Andersson, M., Scharnweber, K. and Eklöv, P. (2024) 'Environmental and ecological drivers of eye size variation in a freshwater predator: A trade-off between foraging and predation risk', *Functional Ecology*, 38(11), pp. 2470–2477.

Bakewell, A. *et al.* (2020) 'Comparing Life Histories across Taxonomic Groups in Multiple Dimensions: How Mammal-Like Are Insects?', *The American Naturalist*, 195, pp. 71–81.

Bernado, C. *et al.* (2024) 'Warming changes the life history composition of marine fish communities at high latitudes', *Marine Ecology Progress Series*, 732, pp. 119–133.

Bielby, J. *et al.* (2007) 'The Fast-Slow Continuum in Mammalian Life History: An Empirical Reevaluation', *The American Naturalist*, 169(6), pp. 748–757.

Brönmark, C. and Miner (1992) 'Predator-Induced Phenotypical Change in Body Morphology in Crucian Carp', *Science*, 258(5086), pp. 1348–1350.

Brosse, S. and Charpin, N. (2021) 'FISHMORPH: A global database on morphological traits of freshwater fishes', *Global Ecology and Biogeography*, 30(12). Available at: https://doi.org/10.1111/geb.13395.

Capdevila, P., *et al.* (2020) 'Longevity, body dimension and reproductive mode drive differences in aquatic versus terrestrial life-history strategies', *Functional Ecology*, 34(8), pp. 1613–1625.

Capdevila, P., *et al.* (2020) 'Towards a Comparative Framework of Demographic Resilience', *Trends in Ecology and Evolution*, 35, pp. 776–786.

Capdevila, P. *et al.* (2021) 'Reconciling resilience across ecological systems, species and subdisciplines', *Journal of Ecology*, 109(9), pp. 3102–3113.

Carruthers, T. *et al.* (2014) 'Evaluating methods for setting catch limits in data-limited fisheries', *Fisheries Research*, 153, pp. 48–66.

Caswell, H. (2001) *Matrix Population Models: Construction, Analysis, and Interpretation*. 2nd edn. Sunderland, Massachusetts: Sinauer Associates.

Charlesworth, B. (1994) *Evolution in Age-Structured Populations*. 2nd edn. Cambridge University Press.

Chea, R. *et al.* (2021) 'Do Morphological Traits Predict Ecological Guilds of the Mekong Fish Fauna?', *Sustainability*, 13(15), p. 8401.

Clement, C., and Ozgul, A. (2016). Including trait-based early warning signals helps predict population collapse. Nature Communications, 7, 10984. https ://doi.org/10.1038/ncomm s10984

CSIRO Australian National Fish Collection (2008) *Greeneye spurdog (Squalus chloroculus)* [Photograph]. Available at: http://hdl.handle.net/102.100.100/706999?index=1.

Elgar, M. (1990) 'Evolutionary compromise between a few large and many small eggs: comparative evidence in teleost fish', *Oikos*, 59(2), pp. 283–287.

Freckleton, R., Harvey, H. and Pagel, M. (2002) 'Phylogenetic Analysis and Comparative Data: A Test and Review of Evidence', *American Naturalist*, 160(6), pp. 712–726.

Froese, R. *et al.* (2020) 'Estimating stock status from relative abundance and resilience', *ICES Journal of Marine Science*, 77(2), pp. 527–538.

Froese, R. and Pauly, D. (2013) 'FishBase'. Available at: www.fishbase.org.

Gaillard, J. *et al.* (1989) 'An analysis of demographic tactics in birds and mammals', *Oikos*, 56, pp. 59–76.

Gaillard, J. *et al.* (2005) 'Generation Time: A Reliable Metric to Measure Life-History Variation among Mammalian Populations', *The American Naturalist*, 166(1).

Gaillard, J. *et al*. 2016. "Life Histories, Axes of Variation in." In *Encyclopedia of Evolutionary Biology*, edited by R. M. Kliman, 312–323. Academic Press.

Gatz, A. (1979) 'Community Organization in Fishes as Indicated by Morphological Features', *Ecology*, 60(4), pp. 711–718.

Gonçalves-Souza, T., Vieira, M. L., Souza, B. D., *et al*. (2023) "A comprehensive review of traits used in functional animal ecology and their predictive power for population performance." *Ecology and Evolution*, 13, e10115901.

Gleiss, A., Potvin, J. and Goldbogen, J. (2017) 'Physical trade-offs shape the evolution of buoyancy control in sharks', *Proceedings of the Royal Society B Biological Sciences*, 284(1866).

Gordon, H. (1954) 'The economic theory of a common property resource: the fishery', *Journal of Political Economics*, 62, pp. 124–142.

Healy, K. *et al.* (2019) 'Animal life history is shaped by the pace of life and the distribution of age-specific mortality and reproduction', *Nature Ecology & Evolution*, 3, pp. 1217–1224.

Heppell, S., Caswell, H. and Crowder, L. (2000) ‘Life histories and elasticity patterns: perturbation analysis for species with minimal demographic data’, 81(3), pp. 654–665.

Houde, E. and Zastrow, C. (1993) ‘Ecosystem-and taxon-specific dynamic and energetics properties of larval fish assemblages’, *Bulletin of Marine Science*, 53(2), pp. 290–335.

Howe, S. (2022) ‘Testing the effects of body depth on fish manoeuverability via robophysical models’, *Bioinspiration & Biometrics*, 17, p. 016002.

Hussey, N. (2009) ‘Maternal investment and size-specific reproductive output in carcharhinid sharks’, *Journal of Animal Ecology*, 79, pp. 184–193.

iNaturalist (2023) ‘iNaturalist’. Available at: https://www.inaturalist.org/ (Accessed: 1 September 2025).

Jeschke, J. and Kokko, H. (2009) ‘The roles of body size and phylogeny in fast and slow life histories’, *Evolutionary Ecology*, 23, pp. 867–878.

Kaiser, H. (1960) ‘The application of electronic computers to factor analysis’, *Educational and Psychological Measurement*, 20, pp. 141–151.

Katona, G. *et al.* (2023) ‘Evolution of reproductive modes in sharks and rays’, *Journal of Evolutionary Biology*, 36(11), pp. 1630–1640.

Kelly, R. *et al.* (2021) ‘Climatic and evolutionary contexts are required to infer plant life history strategies from functional traits at a global scale’, *Ecology Letters*, 24(5), pp. 970–983.

kengraham (2025) *Banded stingaree (Urolophus cruciatus)* [Photograph]. Available at: https://doi.org/10.15468/ab3s5x (Accessed: 7 September 2025).

King, J. and McFarlane, C. (2003) ‘Marine fish life history strategies: Applications to fishery management’, *Fisheries Management and Ecology*, 10(4), pp. 249–264.

Kooijman, S. (2000) *Dynamic Energy Mass Budgets in Biological Systems*. Cambridge: Cambridge University Press.

Lailvaux, S. P. and Husak, J. F. (2014). The life history of whole-organism performance. *The Quarterly Review of Biology*. Biol. 89:285 318.

Lailvaux, S. P. and Husak, J. F. (2017). Predicting life-history trade-offs with whole-organism performance. *Integrative and Comparative Biology* 57:325-331.

Land, M. (1981) ‘Optics and vision in invertebrates’, in *Handbook of Sensory Physiology*. Berling: Springer-Verlag, pp. 471–592.

Laughlin, D. C., *et al*. (2020) The net effect of functional traits on fitness. *Trends in Ecology & Evolution*, 35(11), 1037-1047.

Linsey, T. and Collin, S. (2007) ‘Relative eye size in elasmobranchs’, *Brain, Behavour, and Evolution*, 69(4), pp. 266–279.

Lucas, S. *et al.* (2025) ‘Changing feeding levels reveal plasticity in elasmobranch life history strategies’, *Ecology Letters*, 28(9), p. e70201. Available at: https://doi.org/10.1101/2024.07.11.601909.

Michonneau, F., Brown, J. and Winter, D. (2016) 'rotl: an R package to interact with the Open Tree of Life data', *Methods in Ecology and Evolution*, 7(12), pp. 1476–1481. Available at: https://doi.org/10.1111/2041-210X.12593.

Milla, R. *et al.* (2008) 'Environmental and developmental controls on specific leaf area are little modified by leaf allometry', *Functional Ecology*, 22(4), pp. 565–576.

Morrison, C. and Hero, J.-M. (2003) 'Geographic variation in life-history characteristics of amphibians: a review', *Journal of Animal Ecology*, 72(2), pp. 270–279.

Mouchet, M. *et al.* (2019) 'Using a trait-based approach to understand the efficiency of a selective device in a multispecific fishery', *Scientific Reports*, 9, p. 12489.

Musick, J. (1999) 'Criteria to Define Extinction Risk in Marine Fishes: The American Fisheries Society Initiative', *Fisheries*, 24(12), pp. 6–14.

Myers, E. *et al.* (2019) 'Changes in key traits versus depth and latitude suggest energy-efficient locomotion, opportunistic feeding and light lead to adaptive morphologies of marine fishes', *Journal of Animal Ecology*, 89(2), pp. 309–322.

Neat, F. and Campbell, N. (2013) 'Proliferation of elongate fishes in the deep sea', *Journal of Fish Biology*, 83(6), pp. 1576–1591.

Nilsson, P., Brönmark, C. and Pettersson, L. (1995) 'Benefits of a predator-induced morphology in crucian carp', *Oecologia*, 104, pp. 291–296.

Oli, M. and Dobson, S. (2003) 'The Relative Importance of Life-History Variables to Population Growth Rate in Mammals: Cole's Prediction Revisited', *The American Naturalist*, 161(3).

Ozgul, A. *et al.* (2024) 'Destabilizing effect of climate change on the persistence of a short-lived primate', *Proceedings of the National Academy of Sciences: Population Biology*, 120(14), pp. 1–9.

Pagel, M. (1999) 'Inferring the historical patterns of biological evolution', *Nature*, 401, pp. 877–884.

Paniw, M. *et al.* (2018) 'Life history responses of meerkats to seasonal changes in extreme environments', *Science*, 363(6427), pp. 631–635.

Pardo, S. *et al.* (2016) 'Maximum intrinsic rate of population increase in sharks, rays, and chimaeras: the importance of survival to maturity', *Canada Journal of Fish and Aquatic Science*, 73, pp. 1159–1163.

Pennino, M.G., Coll, M. and Cerviño, S. (2023) 'The challenges of modelling and assessing fisheries resources', *ICES Journal of Marine Science*, 80(10), pp. 2563–2566.

Pianka, E. (1970) 'On r- and K-selection', *The American Naturalist*, 104, pp. 592–597.

Piet, G. and Guruge, W. (1997) 'Diel variation in feeding and vertical distribution of ten co-occurring fish species: consequences for resource partitioning.', *Environmental Biology of Fishes*, 50, pp. 293–307.

Punt, A. (2000) 'Extinction of marine renewable resources: a demographic analysis', *Population Ecology*, 42, pp. 19–27.

R Core Team (2024) 'R: A Language and Environment for Statistical Computing'. Vienna, Austria: R Foundation for Statistical Computing. Available at: https://www.R-project.org/.

Rademaker, M., van Leeuwen, A. and Smallegange, I. (2024) 'Why we cannot always expect life history strategies to directly inform on sensitivity to environmental change', *Journal of Marine Ecology*, 00, pp. 1–19.

Revell, L. (2012) 'phytools: An R package for phylogenetic comparative biology (and other things).', *Methods in Ecology and Evolution*, 3, pp. 217–223.

Reznick, D., Bryga, H. and Endler, J. (1990) 'Experimentally induced life-history evolution in a natural population', *Nature*, 346, pp. 357–359.

Sæther, B.-E. (1987) 'The Influence of Body Weight on the Covariation between Reproductive Traits in European Birds', *Oikos*, 48(1), pp. 79–88.

Salguero-Gómez, R. *et al.* (2016) 'Fast–slow continuum and reproductive strategies structure plant life-history variation worldwide', *Proceedings of the National Academy of Sciences: Population Biology*, 113, pp. 230–235.

Salguero-Gómez, R. (2017) 'Applications of the fast-slow continuum and reproductive strategy framework of plant life histories', *New Phytologist*, 213(4), pp. 1618–1624.

Salguero-Gómez, R. *et al.* (2018) Delivering the promises of trait-based approaches to the needs of demographic approaches, and vice versa, *Functional Ecology*, 32(6), pp. 1424–1435.

Schneider, C., Rasband, W. and Eliceiri, K. (2012) 'NIH Image to ImageJ: 25 years of image analysis', *Nature Methods*, 9(7).

Seibel, B., Thuesen, E. and Childress, J. (2000) 'Light-Limitation on Predator-Prey Interactions: Consequences for Metabolism and Locomotion of Deep-Sea Cephalopods', *Biological Bulletin*, 198(2), pp. 284–298.

Shultz AJ, Adams BJ, Bell KC, Ludt WB, Pauly GB, Vendetti JE. Natural history collections are critical resources for contemporary and future studies of urban evolution. Evol Appl. 2020 Jul 2;14(1):233-247. doi: 10.1111/eva.13045.

Sibly, R. *et al.* (2018) 'The shark-tuna dichotomy: why tuna lay tiny eggs but sharks produce large offspring', *The Royal Society Open Science*, 5(8), p. 180453.

Siefert, A., & Laughlin, D. C. (2023) "Estimating the net effect of functional traits on fitness across species." *Methods in Ecology and Evolution*, 14, 14079

Smallegange, I. *et al.* (2017) 'Mechanistic description of population dynamics using dynamic energy budget theory incorporated into integral projection models', *Methods in Ecology and Evolution*, 8(2), pp. 146–154.

Smallegange, I., Edwards, L. and Attle, A. (2025) 'Population Performance and Resilience in Polychaetes as Environmental Indicators of Estuarine Ecosystems', in *Estuaries - Dynamic Ecosystems at the Land-Sea Interface [Working Title]*. IntechOpen. Available at: http://dx.doi.org/10.5772/intechopen.1011169.

Smallegange IM, Berg M. 2019. A functional trait approach to identifying life history patterns in stochastic environments. Ecology and Evolution 9: 9350-9361

Smallegange, I. and Lucas, S. (2024) 'DEBBIES Dataset to study Life Histories across Ectotherms', *Scientific Data*, 11, p. 153.

Stahl, J. and Oli, M. (2006) 'Relative importance of avian life-history variables to population growth rate', *Ecological Modelling*, 198, pp. 23–39.

Stearns, S. (1992) *The Evolution of Life Histories*. London, England: Oxford University Press.

Stearns, S. (2000) 'Life history evolution: successes, limitations, and prospects', *Naturwissenschafte*, 87, pp. 476–486.

Stott, I. *et al.* (2024) 'Life histories are not just fast or slow', *Trends in Ecology and Evolution*, 39(9), pp. 830–841.

Stott, I., Townley, S. and Hodgson, D. (2011) 'A framework for studying transient dynamics of population projection matrix models', *Ecology Letters*, 14(9), pp. 959–970.

Swenson, N. G., Worthy, S., Eubanks, D., et al. (2019) A reframing of trait–demographic rate analyses for ecology and evolutionary biology. *International Journal of Plant Sciences*, 181(1), 706189.

The MathWorks Inc (2024) 'MATLAB'. Available at: https://www.mathworks.com.

Tytell, E. *et al.* (2010) 'Disentangling the Functional Roles of Morphology and Motion in the Swimming of Fish', *Integrative and Comparative Biology*, 50(6), pp. 1140–1154.

Villéger, S. *et al.* (2010) 'Contrasting changes in taxonomic vs. functional diversity of tropical fish communities after habitat degradation', *Ecological Applications*, 20(6), pp. 1512–1522.

Villéger, S. *et al.* (2017) 'Functional ecology of fish: Current approaches and future challenges', *Aquatic Sciences*, 79, pp. 783–801.

Violle, C. *et al.* (2007) 'Let the concept of trait be functional!', *Oikos*, 116(5), pp. 882–892.

Webb, P. (1984) 'Body Form, Locomotion and Foraging in Aquatic Vertebrates', *American Zoologist*, 24, pp. 107–120.

Wickham, H. (2007) 'Reshaping Data with the reshape Package', *Journal of Statistical Software*, 21(12), pp. 1–20.

Wickham, H. (2016) *ggplot2: Elegant Graphics for Data Analysis*. New York: Springer-Verlag. Available at: https://ggplot2.tidyverse.org.

Wieczynski, D. J., Dietrich, J., Dickens, B., Sears, A., Gomez, A., ... (2021) Linking species traits and demography to explain complex temperature responses across levels of organization. Proceedings of the National Academy of Sciences of the United States of America, 118(37): e2104863118

Winemiller, K. (1989) 'Patterns of variation in life history among South American fishes in seasonal environments', *Oecologia*, 81, pp. 225–241.

Winemiller, K. (2005) 'Life history strategies, population regulation, and implications for fisheries management', *Canadian Journal of Fisheries and Aquatic Sciences*, 62(4), pp. 872–885.

Winemiller, K. and Rose, K. (1993) 'Why do most fish produce so many tiny offspring?', *American Naturalist*, 142(4), pp. 585–603.

Zhang, M., Fouhey, D. F. (2022) A deep neural network for high-throughput measurement of functional traits on museum skeletal specimens. Methods in Ecology and Evolution, 14, 347-359.

Table 1: Life history traits calculated from the DEB-IPMs with their definition and how they were calculated. The final two columns are the scores for each of the life history traits on a phylogenetically and length corrected principal component analysis (LH-pPCA). Significant traits for each of the axes (score > 0.5) are in bold. The traits for LH-pPC1 are associated with generation turnover and the traits for LH-pPC2 are associated with reproductive output.

Life history traits				*Length corrected pPCA*	
Life history trait	**Symbol**	**Definition**	**Equation**	**LH-pPC1**	**LH-pPC2**
Generation time	T	Number of years required for the individuals of a population to be fully replaced by new ones	$T = \frac{log\ (R_0)}{log\ (\lambda)}$	**-0.9295**	0.0517
Age at maturity	L_α	Number of years that it takes an average individual in the population to become reproductive	$L_\alpha = \eta_{L_b}$	**-0.6009**	**0.6463**
Progressive growth	g	Mean probability of growing to a larger length across the length domain W.	$\gamma = \sum_{i}^{m} \underline{G}_{i,j}\|_{i<j}$	**-0.7579**	0.0884
Retrogressive growth	r	Mean probability of growing to a smaller length across the length domain W.	$\rho = \sum_{i}^{m} \underline{G}_{i,j}\|_{i>j}$	-0.3391	**-0.7753**
Mean recruitment success	j	Mean per-capita number of recruits across the length domain W.	$\varphi = \sum_{i}^{m} \underline{V}_{i,j}$	**0.8191**	0.4879
Degree of iteroparity	S	Coefficient of variation in age at reproduction	$S = \frac{\underline{m}_x}{\sigma(m_x)}$	0.4534	0.1920
Net reproductive rate	R_0	Mean number of recruits produced during the mean life expectancy of an individual in the population.	$R_0 = \sum_{x=0}^{x=\eta_e} l_x m_x$	0.1678	**0.9526**
Mature life expectancy	L_ω	Number of years from the mean age at maturity (L_α) until the mean life expectancy (η_e) of an individual in the population.	$L_\varpi = \eta_{L_p}$	**-0.6844**	**0.5932**
Axis – named by trait associations				**Turnover**	**Output**
Proportion of variance explained				41.09%	32.04%
Cumulative proportion of variance explained				41.09%	73.14%
Kaiser criterion				3.28	2.56
Pagel's lambda (λ_p)				0.98	

Afte After Smallegange & Lucas (2024): to calculate life history traits, we discretised the IPM by dividing the length domain Ω into very small-width discrete bins (we chose 200 bins), resulting in a matrix **A** of size $p \times q$, where $p = q = 200$, and which dominant eigenvalue equals λ, the population growth rate. Mean lifetime reproductive success R_0 is the dominant eigenvalue of the matrix $\mathbf{F} = \mathbf{V}(\mathbf{I} - \mathbf{GS})^{-1}$, where **I** is the identity matrix and **V** = **DR**, with **D** as the parent-offspring association, **R** the reproduction, **G** the growth and **S** the survival matrix; this gives generation time $T = \log(R_0)/\log(\lambda)$. The mean life expectancy, η_e, is calculated as $\eta_e = \mathbf{1}^{\mathrm{T}}\mathbf{N}$, where **1** is a vector of ones of length m and **N** is the fundamental matrix $\mathbf{N} = (\mathbf{I} - \mathbf{S})^{-1}$. The longevity of an individual of length L is η_L, which means we can calculate age at sexual maturity $t_p = \eta_{L_b}$ and mature life expectancy $L_\varpi = \eta_{L_p}$ so that $\eta_e = t_p + L_\varpi$. l_x is the probability of surviving to age at least x, and m_x is the average fertility of age class x. $\overline{\mathbf{G}}$ is the mean of **G**, $\overline{\mathbf{V}}$ is the mean of **V,** and i and j are the row and column entries of the matrix, respectively. The vital rates included in progressive growth γ, retrogressive growth ρ, and sexual reproduction ϕ, were averaged across the columns j (the length bins), weighted by the relative contributions of each stage at stationary equilibrium. For example, to calculate mean sexual reproduction ϕ, we summed the values in the columns j of the **V** matrix and multiplied each ϕ_{ij} by the corresponding jth element w_j of the stable stage distribution **w**, calculated as the right eigenvector of **A**. Finally, the degree of iteroparity $S = \sqrt{V_{\mathbf{f}}}/\bar{a}_{\mathbf{f}}$, with $V_{\mathbf{f}} = \overline{a_{\mathbf{f}}^2} - (\bar{a}_{\mathbf{f}})^2$, where $\overline{a_{\mathbf{f}}^2} = [(\mathbf{c} \circ \mathbf{c})^{\mathrm{T}} \otimes \sum_{x=0}^{x=\eta_e} m_x]/[\mathbf{1}^{\mathrm{T}} \otimes \sum_{x=0}^{x=\eta_e} m_x]$ and $\bar{a}_{\mathbf{f}} = [\mathbf{c}^{\mathrm{T}} \otimes \sum_{x=0}^{x=\eta_e} m_x]/[\mathbf{1}^{\mathrm{T}} \otimes \sum_{x=0}^{x=\eta_e} m_x]$, with $\mathbf{c}^{\mathrm{T}} = (1\ 2\ \cdots\ p)$.

Table 2: Description and diagram of trait measurements for a ray-finned fish taken from lateral view images (adapted from Brosse and Charpin (2021)). Measurements introduced in this study, Caudal fin inner fork distance (CFi) and Caudal fin outer fork distance (CFo) are defined below and highlighted in blue in the figure, along with the other measurements.

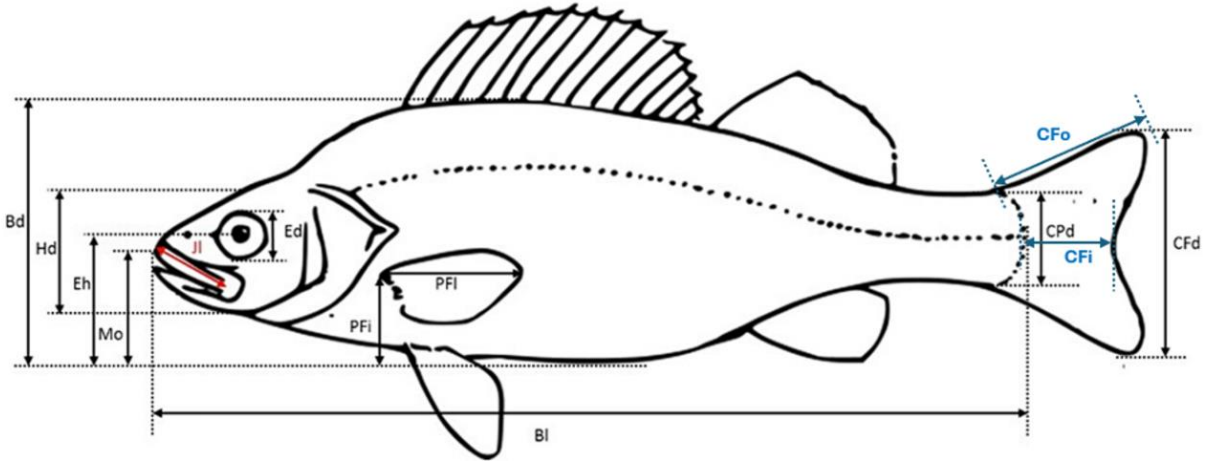

Code	Name	Protocol for measurement
BL	Body length	Standard length (snout to caudal fin base)
Bd	Body depth	Maximum body depth
Hd	Head depth	Head depth at the vertical of the eye
CPd	Caudal peduncle depth	Minimum depth of the caudal peduncle
CFd	Caudal fin depth	Maximum depth of the caudal fin
Ed	Eye diameter	Vertical diameter of the eye
Eh	Eye position	Vertical distance between the centre of the eye and the bottom of the body
Mo	Mouth height	Vertical distance from the top of the mouth to the bottom of the body
Jl	Maxillary jaw length	Length from snout to the corner of mouth
PFl	Pectoral fin length	Length of the longest ray of the pectoral fin
PFj	Pectoral fin position	Vertical distance between the upper insertion of the pectoral fin to the bottom of the body
CFi	Caudal fin inner fork distance	Beginning of caudal fin (from the lateral line of the spine) to the divide between the upper and lower lobes
CFo	Caudal fin outer fork distance	Beginning of caudal fin (from the top of the body) to the furthest tip of the upper lobe

Table 3: List of the morphological trait ratios included in the morphological PCA, their definitions and how they were calculated (see Table 2). The final three columns show the results of the phylogenetically and length corrected PCA (M-pPCA). Traits that had significant loadings (>0.5) are highlighted in bold. M-pPC axes were names based on the associations of their significant traits: M-pPC1 is related to body size, M-pPC2 is associated with manoeuvring, M-pPC3 is associated with position in the water column relative to prey/predators.

Morphological traits				*Length corrected pPCA*		
Morphological trait	**Symbol**	**Definition**	**Equation**	**M-pPC1**	**M-pPC2**	**M-pPC3**
Body elongation	BEl	Length of the body relative to its depth; linked with hydrodynamism	$\frac{Bl}{Bd}$	**-0.52**	**0.70**	0.16
Vertical eye position	VEp	Vertical position of the centre of the eye relative to head depth; linked with position in the water column	$\frac{Eh}{Hd}$	-0.46	-0.18	**-0.73**
Relative eye size	REs	Size of the eye relative to the head depth; linked to visual acuity	$\frac{Ed}{Hd}$	**-0.71**	-0.17	0.31
Oral gape position	OGp	Vertical position of the top of the mouth relative to the head depth	$\frac{Mo}{Bd}$	**-0.52**	**-0.58**	-0.17
Body lateral shape	BLs	Difference in depth between the head and the widest part of the trunk	$\frac{Hd}{Bd}$	0.44	0.21	-0.29
Pectoral fin position	PFv	Vertical position of the uppermost insertion of the pectoral fin relative to the depth of the body	$\frac{PFi}{Bd}$	-0.27	0.10	**-0.66**
Pectoral fin size	PFs	The size of the pectoral fin (the longest ray) in relation to the length of the body	$\frac{PFl}{Bl}$	0.49	**-0.74**	-0.05
Caudal fin forkedness	CFk	Distance between the start of the caudal fin to the medium notch relative to the length of the fin's upper lobe to define the forkedness/roundedness of the fin	$\frac{CFi}{CFo}$	-0.33	-0.46	0.447
Axis – named by trait associations				**Lateral**	**Locomotory**	**Positioning**
Proportion of variance explained				23.42%	21.15%	17.35%
Cumulative proportion of variance explained				23.42%	44.58%	61.93%
Kaiser criterion				1.87	1.69	1.38

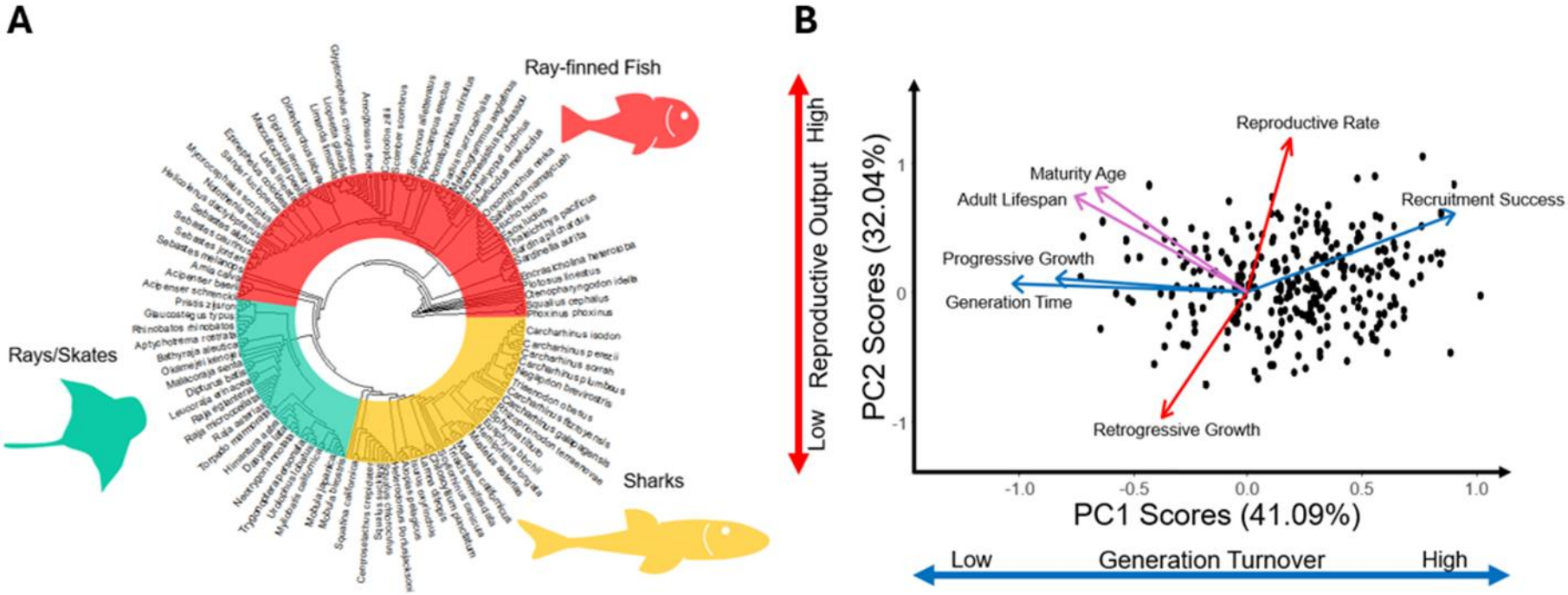

Figure 1. Fish phylogenetic tree and life history biplot. A: Circular phylogenetic tree of the 290 study species across three clades: ray-finned fish (red), rays/skates (green), and sharks (yellow). Branch lengths are derived from The Open Tree of Life. A limited number of tip labels are matched to the tree tips given limited space. **B**: A phylogenetically and length corrected PCA biplot of the life histories of 290 fishes (each species is a solid symbol). The strength of the trait loadings onto each of the axes are shown by the length and direction of the black arrows.

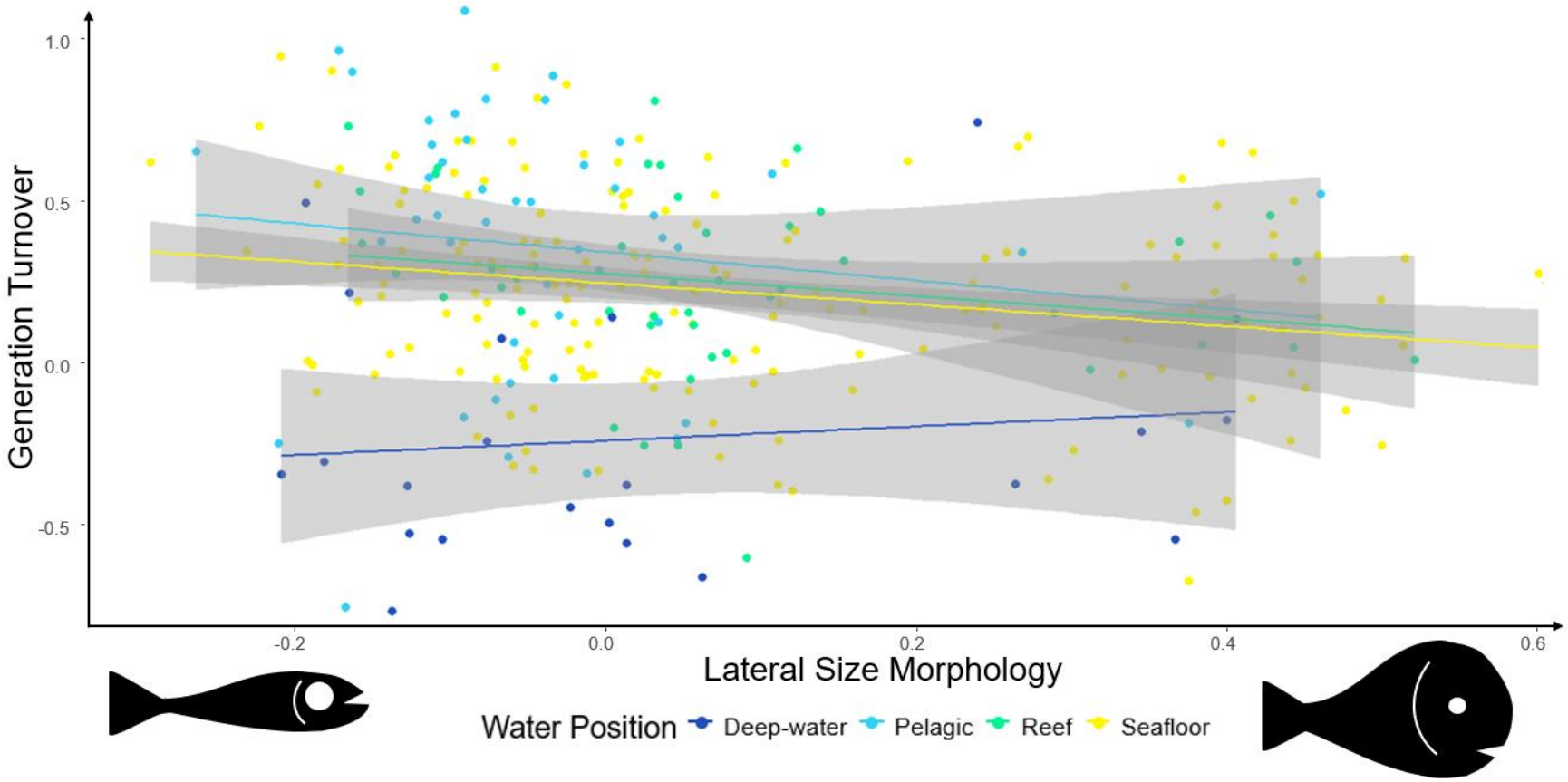

Figure 2: Lateral size morphology predicts generation turnover across different water positions. Scatter plot showing how lateral size morphology predicts generation turnover principal component scores differently depending on species position in the water column (grey areas denote 95% confidence intervals). The fish shadows indicate the scale for lateral size morphology from an elongated form with larger relative eye size and high oral gape position (left) to a rounder form with smaller eyes relative to the head and a low oral gape position (right).

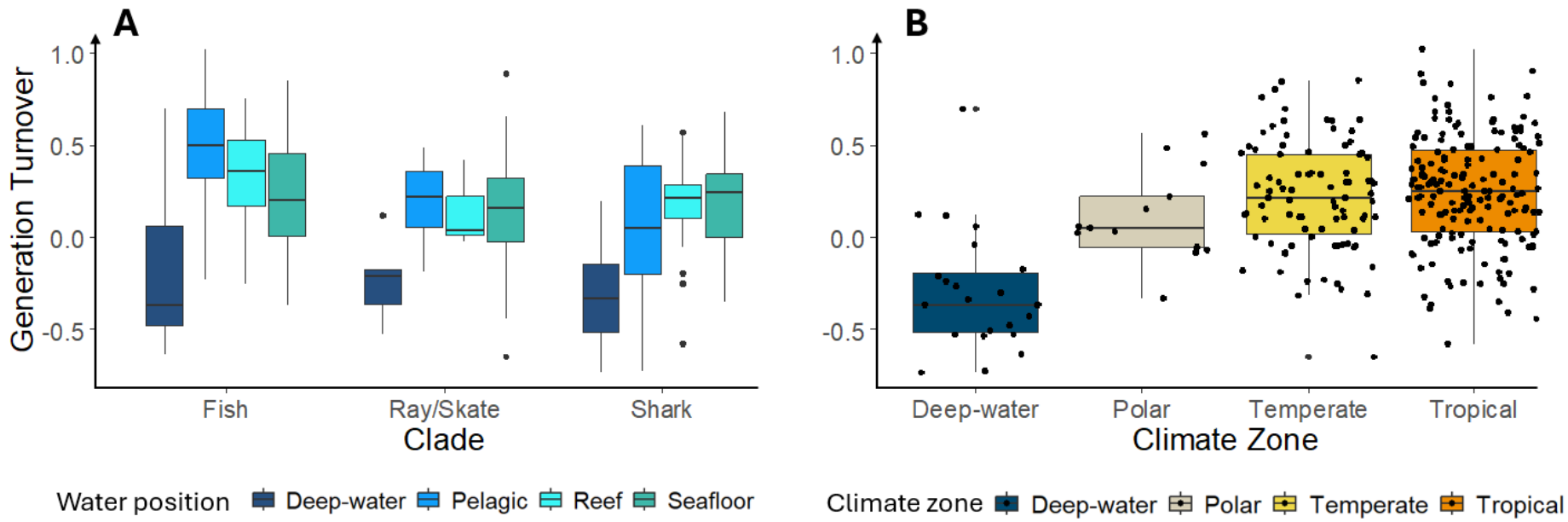

Figure 3: Generation turnover predicted by water position interacting with clade and climate zone. A: Boxplots showing how generation turnover principal component (PC) scores vary between ray-finned fish, rays/skates and sharks across different water positions (black dots are outlier species). **B**: Boxplots showing how generation turnover PC scores changes between deep-water, polar, temperate and tropical climate zones (black dots are species). In both A and B, vertical lines represent the range and horizontal lines of the boxplots are the medians.

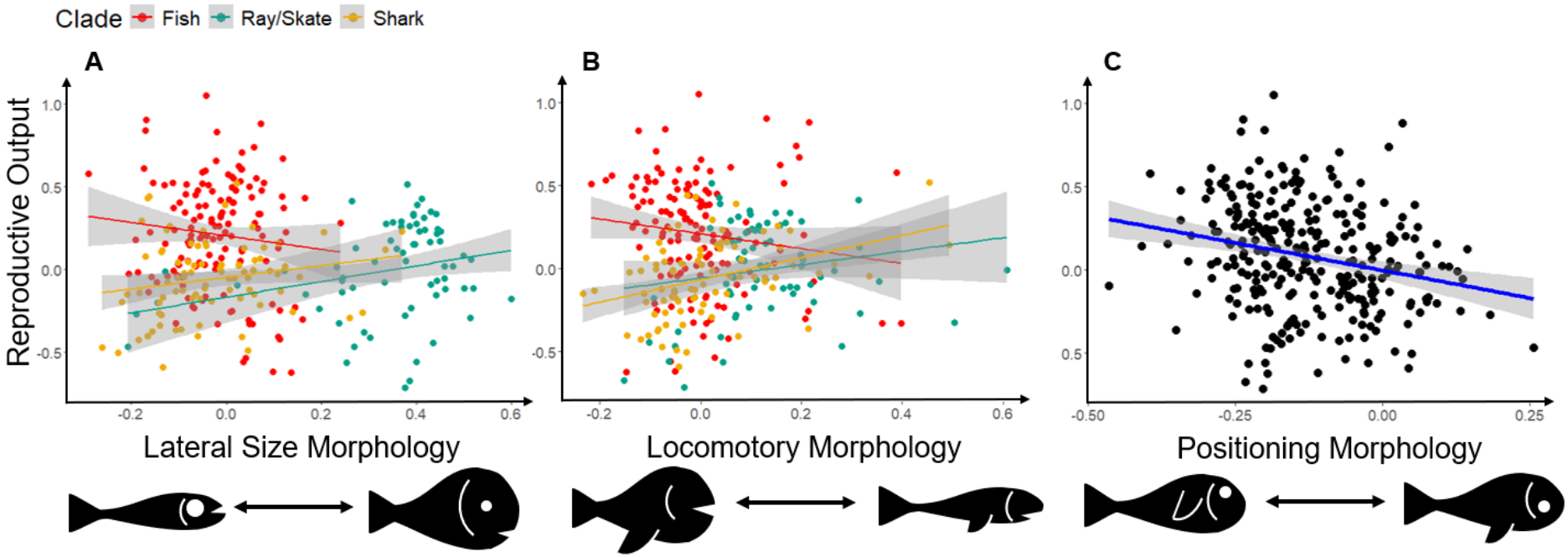

Figure 4: Composite morphological traits predict reproductive output. Scatter graphs showing how each of the morphological principal component (PC) axes scores predict reproductive output either interacting with clade (**A**, **B**) or independently (**C**). Each morphological axis is exemplified with fish shadows showing differences in body elongation, relative eye size, oral gape position, pectoral fin size and pectoral fin position. The linear relationships are shown by coloured lines which match the different clades (red=ray-finned fish, green=rays/skates, yellow=sharks), or are blue if no interactions were significant, and the grey shaded areas represent 95% confidence intervals.

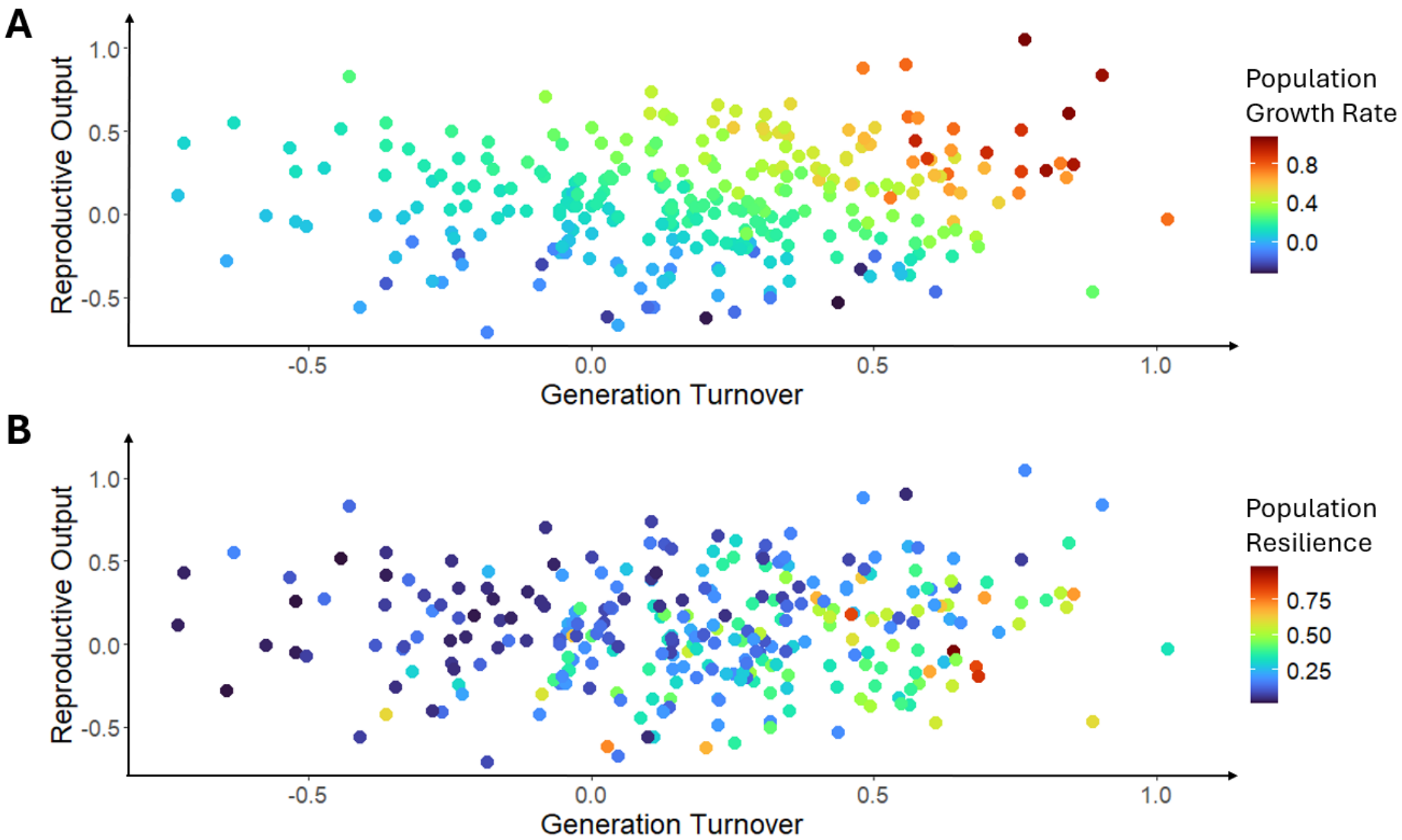

Figure 5: Population growth rate and resilience. Overlays on the biplots demonstrating (**A**) how population growth rate (λ_0) increases with increasing generation turnover and reproductive output principal component (PC) scores, and (**B**) how demographic resilience changes with turnover and output. Values of λ_0 and resilience range from high (red) to low (blue). Each point represents one species.

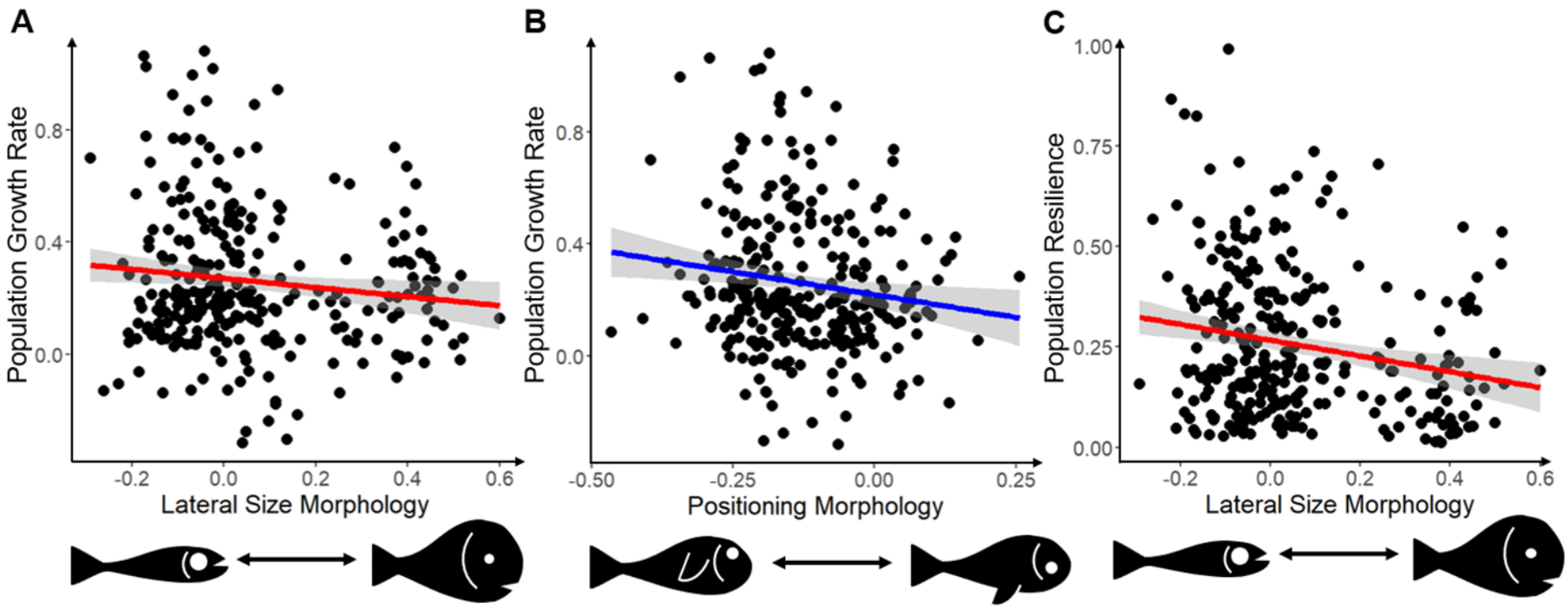

Figure 6: Morphology predicts population growth rate and resilience. Scatter plots demonstrating how the morphological principal component (PC) scores predict population growth rate (**A**, **B**) and population resilience (**C**). Each morphological axis is exemplified with fish shadows showing differences in body elongation, relative eye size, oral gape position and pectoral fin size. The linear relationships are shown by coloured lines which match the morphological axes (red=lateral size morphology, blue=positioning morphology) and the grey shaded areas are 95% confidence intervals.